HEAT TRANSFER IN HIGH-TEMPERATURE MULTILAYER INSULATION

Kamran Daryabeigi,[(1)] Stephen D. Miller,[(2)] George R. Cunnington[(3)]

[(1)] NASA Langley Research Center, Hampton, Virginia, U.S.A. Email: kamran.daryabeigi-1@nasa.gov
[(2)] SD Miller and Associates Research Foundation, Flagstaff, Arizona, U.S.A. Email: smiller@samrf.org
[(3)] Cunnington and Associates, Palo Alto, California, U.S.A. Email: grcunn@comcast.net

ABSTRACT

The combined radiation/conduction heat transfer in high-temperature multilayer insulations for typical reentry of reusable launch vehicles from low Earth orbit was investigated experimentally and numerically. The high-temperature multilayer insulation investigated consisted of gold-coated reflective foils separated by alumina fibrous insulation spacers. The steady-state heat transfer through four multilayer insulation configurations was investigated experimentally over the temperature range of 300-1300 K and environmental pressure range of 1.33×10^{-5}-101.32 kPa. It was shown that including the reflective foils reduced the effective thermal conductivity compared to fibrous insulation sample at 1.5 times the density of the multilayer sample. A finite volume numerical model was developed to solve the governing combined radiation/conduction heat transfer equations. The radiation heat transfer in the fibrous insulation spacers was modeled using the modified two-flux approximation assuming anisotropic scattering and gray medium. The numerical model was validated by comparison with steady-state experimental data. The root mean square deviation between the predicted and measured effective thermal conductivity of the samples was 9.5%.

Nomenclature

b = back scattering fraction
c = specific heat, J/(kg.K)
e = specific extinction coefficient, m^2/kg
F^+ = forward radiative flux, W/m^2
F^- = backward radiative flux, W/m^2
f = solid fraction ratio
K_B = Boltzmann constant, 1.3806×10^{-23} J/K
Kn = Knudsen number
k = thermal conductivity, W/(m.K)
L = insulation/spacer thickness, m
n = index of refraction
P = pressure, Pa
Pr = Prandtl number
q'' =. heat flux, W/m^2
T = temperature, K
t = time, s
x = spatial coordinate, m
α = thermal accommodation coefficient
β = extinction coefficient, 1/m
γ = specific heat ratio
ε = emittance
ρ = density, kg/m^3
σ = Stefan-Boltzmann constant, 5.67×10^{-8} $W/(m^2.K^4)$
τ_o = optical thickness
ω =. albedo of scattering

Subscripts
e = effective property
g = gas
r = radiation
s = solid

Superscripts
* = property at atmospheric pressure
** = property of parent material

1. INTRODUCTION

A thermal protection system (TPS) is used to maintain the aerospace vehicle's structural temperature within acceptable limits during reentry flight into Earth's atmosphere, or during sustained flight of hypersonic vehicles. Various insulation concepts can be used to provide the thermal protection function. Rigid ceramic tiles and blanket insulations have been used on the Space Shuttle Orbiter [1], while metallic thermal protection systems were considered for the X-33 vehicle [2], reusable launch vehicles [3], and hypersonic vehicles [4]. Ceramic matrix composite (CMC) TPS have also been investigated for reentry applications [5], and are similar to metallic TPS, but use CMC components which have a higher temperature capability. Metallic and CMC TPS, and blankets can utilize various types of non-load bearing insulations. In most cases non-rigid fibrous insulation has been used or proposed. The use of high-temperature multilayer insulations (MLI) for use in either blanket, metallic or CMC TPS is the subject of this investigation.

The high-temperature MLI typically consists of thin ceramic foils with high reflectance coatings separated by fibrous insulation spacers. A photograph of a typical high-temperature MLI using gold-coated reflective foils and alumina fibrous insulation spacers is shown in Figure 1.

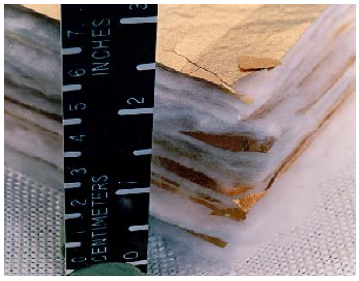

Fig. 1 Photograph of a high-temperature MLI

Low-temperature MLI's have had considerable research and development, and have been widely used for satellite/spacecraft and cryogenic applications [6]. The surface temperatures, instantaneous heating rates, and integrated heating loads for low-temperature MLI are relatively low. Because these MLI typically operate in vacuum, either at low pressures in space, or are maintained in hermetically sealed enclosures, the main modes of heat transfer in these insulations are radiation and solid conduction, with the radiation being dominant. These designs typically rely on using a significant number of closely spaced highly reflective thin foils separated by either thin fibrous insulation spacers, various nettings, or by using integral spacers such as crinkling or dimpling the foils. In most designs the spacers are simply used to ensure the various foils do not touch each other, and maintain the desired spacing between the foils. The radiation heat transfer between successive highly reflective foils then provides the necessary thermal resistance to heat transfer through these MLI. The use of thin fibrous insulation spacers ensures that the optical thickness of the spacers in the in-plane direction is sufficiently high to minimize lateral radiation heat losses. Cunnington and Tien performed a detailed study of heat transfer process in cryogenic MLI's for spacecraft [7]. The low-temperature MLI designs are typically for quasi steady-state or short transient heating applications, therefore, they mainly rely on the low effective thermal conductivity of the MLI to perform the TPS function, and do not have stringent requirements on having sufficient thermal mass for meeting the transient heating requirements.

The MLI's for reentry applications have much higher surface temperatures, and higher heating rates and integrated heating loads. Furthermore, reentry is a long transient heating process, therefore, requiring sufficient thermal mass to ensure that the underlying structure doesn't exceed its design temperature limits. Heat transfer through a high-temperature MLI during atmospheric reentry involves combined modes of heat transfer: radiation, solid and gas conduction. If the density of fibrous insulation spacers is greater then 20 kg/m^3, natural convection can be ignored as a mode of heat transfer [8]. The pressure inside the MLI closely follows the environmental pressure during reentry, going from very low pressures at reentry to atmospheric pressure at landing. Hermetically sealing or encapsulating MLI for reentry is expensive and could result in increasing the overall TPS risks if the encapsulation develops a leak and can not maintain the pressure inside the encapsulation enclosure at vacuum conditions. For a vented high-temperature MLI, the dominant modes of heat transfer are radiation and gas conduction. The relative significance of the different modes of heat transfer varies throughout the thickness of the insulation and is a strong function of temperature and pressure. The high-temperature MLI uses fibrous insulation spacers between the reflective foils. The spacers serve two functions: attenuate radiation between the foils, and provide sufficient thermal mass in order to withstand the highly transient heating loads.

Cunnington, et al. [9] measured the effective thermal conductivity of MLI's at temperatures up to 700 K and at a pressure of 1.33×10^{-3} Pa, and used the optically thin approximation for the modeling the radiation heat transfer. DeWitt, et al. [10] performed experimental measurements to 1273 K at a pressure of 0.133 Pa, and provided a theoretical formulation by neglecting gas conduction and modeling radiation using the optically thick approximation. Mühlratzer, et al. [11] discussed the feasibility of using a metallic TPS with MLI for hypersonic space transportation. Keller and his colleagues also provided various theoretical models of heat transfer in MLI where they neglected solid conduction and used either the optically thick or the modified diffusion approximation for modeling the radiation transfer [12, 13]. Stauffer, et al. [14] provided a theoretical formulation of MLI using the optically thin approximation for the radiation transfer, and compared their predictions with previously published experimental results. Most of the proposed high-temperature MLI designs followed the low-temperature MLI designs by using uniformly-spaced foils throughout the insulation thickness. Daryabeigi [15] used the two flux radiation modeling with isotropic scattering, and optimized the location of reflective foils throughout the insulation thickness for a typical reentry application. The objective of the present work is to extend the previously mentioned work by utilizing two-flux radiation model with anisotropic scattering, and to validate the model with steady-state experimental data on four MLI samples.

2. DESCRIPTION OF MULTILAYER SAMPLES

Four MLI samples were investigated in this study. The MLI samples consisted of gold-coated reflective foils separated by layers of Saffil™ fibrous insulation, a high purity polycrystalline alumina fibrous insulation. The

foils were 152.4 x 152.4 x 0.0104 mm. Each foil consisted of a proprietary substrate coated with gold on both sides. For the samples tested in this study, the nominal gold coating thickness on each side of the foil was 1×10^{-6} m thick. The density of the foils varied between 5175 and 6500 kg/m^3, with the variation in density caused by variations in thicknesses of the gold coating on the different foils. The four MLI samples had a nominal density of 48 kg/m^3. A listing of the thickness, density, and number of foils used in each MLI sample is provided in Table 1. Sample 1 had a thickness of 13.3 mm with four reflective foils, approximately uniformly spaced throughout the thickness of the sample. The other three samples were 26.6 mm thick. Sample 2 was assembled by adding additional alumina fibrous insulation at the bottom of sample 1 to bring its thickness up to 26.6 mm. Therefore, it had four foils located in the upper half of its height. Sample 3 was assembled by removing two of the foils from sample 2, and adding additional alumina fibrous insulation at the bottom of the stack to maintain the same nominal density. Sample 4 was assembled by removing one foil from sample 3, and adding additional alumina fibrous insulation at the bottom of the stack to maintain the same nominal density. A schematic of the four MLI samples is provided in Figure 2. The actual stack-up of the four samples is provided in Table 2.

Table 1. Listing of MLI samples

Sample No.	Thickness (mm)	Density (kg/m^3)	Number of foils
1	13.3	47.3	4
2	26.6	48.2	4
3	26.6	48.3	2
4	26.6	48.4	1

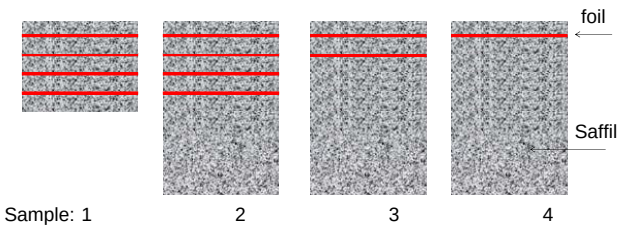

Fig. 2 Schematic of the four MLI samples

Table 2. Stack-up of MLI samples

Fibrous Spacer Number	Thickness (mm), density (kg/m^3)			
	Sample 1	Sample 2	Sample 3	Sample 4
1	2.41, 29.4	1.80, 39.4	1.68, 43.4	1.57, 46.2
2	2.49, 29.4	1.88, 38.9	1.73, 43.6	25.04, 45.9
3	2.49, 29.2	1.85, 39.2	23.22, 43.2	
4	2.57, 29.4	1.93, 39		
5	3.25, 29.3	19.13, 39.2		

3. THERMAL TESTING APPARATUS

A thermal conductivity apparatus [16] was used to measure the steady-state effective thermal conductivity of the MLI samples. The apparatus followed the general guidelines from ASTM standard C201 [17]. In this set-up one side of the test sample was exposed to temperatures in the range of 373 to 12730 K, while the other side was maintained at room temperature, thus providing effective thermal conductivities with temperature differences of 100 to 1000 K maintained across the test sample thickness. This test set–up was not intended for measuring thermal conductivities of the test specimen subjected to small temperature differences maintained across the sample as is customary in the majority of steady-state thermal conductivity measurement techniques. The main purpose was to use a steady-state testing facility for characterization of the thermal performance of the insulation. The results are presented as effective thermal conductivity, even though the results could have also been presented as total heat flux.

The sample to be tested was located between a septum panel and a water-cooled plate. The effective thermal conductivity of the sample was measured with septum panel set at nominal temperatures between 373 and 1273 K, and with the water-cooled plate maintained around room temperature. The apparatus was located inside a vacuum chamber and the environmental pressure was varied between 1.33×10^{-5} and 100 kPa. All the tests were conducted in a gaseous nitrogen environment. Data were typically obtained with nominal temperature differences of 80, 400, 740, and 950 K maintained across the sample thickness and with environmental pressures of 1.33×10^{-5}, 1.33×10^{-4}, 1.33×10^{-3}, 1.33×10^{-2}, 0.033, 0.066, 0.133, 0.333, 0.667, 1.33, 13.33, and 100.32 kPa. The effective thermal

conductivity was calculated using the Fourier law of heat conduction using the following measured average parameters: septum panel temperature, T_1, water-cooled plate temperature, T_2, heat flux on the water-cooled plate, q″, and sample thickness, L, according to:

$$k_e = \frac{q''L}{T_1 - T_2} \tag{1}$$

The average uncertainty of the effective thermal conductivity measurements was 7.5% over the entire range of pressures and temperatures [16].

4. ANALYTICAL HEAT-TRANSFER MODEL

In the absence of natural convection, the governing conservation of energy equation for the problem of combined radiation/conduction in a radiation participating media bounded by two solid surfaces at specified temperatures is given by [18]:

$$\rho c \frac{\partial T}{\partial t} = \frac{\partial}{\partial x}\left(k \frac{\partial T}{\partial x}\right) - \frac{\partial q_r''}{\partial x} \tag{2}$$

subject to the following initial and boundary conditions:

$$T(x, 0) = T_0(x) \tag{3.a}$$
$$T(0,t) = T_1(t) \tag{3.b}$$
$$T(L,t) = T_2(t) \tag{3.c}$$

The modified two-flux approximation was used for modeling the radiation heat transfer in the participating media. Assuming a homogeneous and gray medium, and diffuse emitting/reflecting surfaces, the radiant flux is assumed to be composed of the forward and backward radiative fluxes:

$$q_r'' = F^+ - F^- \tag{4}$$

where the forward and backward radiative fluxes are governed by:

$$\frac{1}{\sqrt{3}\beta}\frac{\partial F^+}{\partial x} = -\left[1-\omega(1-b)\right]F^+ + b\omega F^- + (1-\omega)n^2\sigma T^4 \tag{5.a}$$

$$-\frac{1}{\sqrt{3}\beta}\frac{\partial F^-}{\partial x} = -\left[1-\omega(1-b)\right]F^- + b\omega F^+ + (1-\omega)n^2\sigma T^4 \tag{5.b}$$

This formulation assumes anisotropic scattering and has been used by Domoto and Wang [19] for radiative transfer in gases with anisotropic particle scattering, and by Mathews, et al. [20] for solving the combined radiation/conduction heat transfer in porous materials. The radiant boundary conditions are:

$$F^+(0) = \varepsilon_1 n^2 \sigma T_1^4 + (1-\varepsilon_1)F^-(0) \tag{5.c}$$
$$F^-(L) = \varepsilon_2 n^2 \sigma T_2^4 + (1-\varepsilon_2)F^+(L) \tag{5.d}$$

where the subscripts 1 and 2 refer to the bounding surfaces at $x = 0$ and $x = L$, respectively. The governing equations and boundary conditions given in Eqs. (5.a)-(5.d) constituted a system of first order differential equations, which had to be solved for each fibrous insulation spacer region between two adjacent reflective foils, or between a foil and the bounding solid surface. The index of refraction for alumina fibrous insulation was assumed to be unity [21]. The extinction coefficient is related to the specific extinction coefficient through [22]:

$$\beta = e\rho \tag{6}$$

Gas thermal conductivity does not vary with pressure but the exchange of heat from gas molecules to adjacent solid surfaces (fibers and foils) is influenced by the environmental pressure in the rarefied and transition flow transport regimes. Thus, an effective gas thermal conductivity was defined as [23]:

$$k_g = \frac{k_g^*}{\phi + 2\varphi \frac{2-\alpha}{\alpha}\frac{2\gamma}{\gamma+1}\frac{Kn}{\mathrm{Pr}}} \tag{7}$$

which relates the effective gas thermal conductivity at various pressures to the gas thermal conductivity at atmospheric pressure, k_g^*. The parameters ϕ and ψ depend on the Knudsen number. $\phi = 1$, $\psi = 0$ for Knudsen number less than 0.01 (continuum regime), $\phi = 1$, $\psi = 1$ for Knudsen number between 0.01 and 10 (transition regime), and $\phi = 0$, $\psi = 1$ for Knudsen number greater than 10 (free-molecular regime). The thermal accommodation coefficient for interchange between the alumina fibers and surrounding gas was assumed to be unity.

Theoretical modeling of solid conduction through fibers and points of contact between them is difficult, and various empirical relations have been developed to model the solid conduction. The empirical model used in this study was [8]:

$$k_s = f^{1.469} k_s^{**} \tag{8}$$

which relates the solid thermal conductivity of fibrous insulation to the thermal conductivity of the fiber parent material (alumina), k_s^{**}. The parallel thermal network model was used for modeling the interaction between

solid and gas conduction. This model has been used for modeling heat transfer in rigid [24] and loose fibrous insulations [8]:

$$k = fk_s + (1-f)k_g \quad (9)$$

All the thermophysical properties required for the numerical solution were obtained from published data in the literature, with the exception of the following radiation parameters: albedo of scattering, ω, backscattering fraction, *b*, and specific extinction coefficient, *e*. This overall formulation has been previously applied to a large set of steady-state thermal data on alumina fibrous insulation samples at various densities (24, 48, and 72 kg/m^3) and thicknesses (13.3, 26.6 and 39.9 mm), and found that the following parameter estimates provided a satisfactory match of the experimental results [8]: ω = 0.974, b = 0.268, and e = 53.017+0.03879 T.

The finite volume form of the conservation of energy equation, Eq. (2), was solved using an implicit time marching formulation. Constant temperature boundary conditions were used for specifying data from the steady-state thermal conductivity measurements. The reflective foils were treated as lumped masses in the conservation of energy equation, assuming that there was no significant temperature drop across the thickness of the foils. Eq. (9) was used to model the combined gas/solid conduction term in the fibrous insulation spacers with the solid conduction contribution from Eq. (8), and the gas conduction contribution from Eq. (7). At each time step and for each fibrous insulation spacer region, the radiative heat transfer equations, Eqs. (5.a) - (5.d), were solved using a finite difference technique using the predicted temperature distribution in the medium from the previous time step solution of conservation of energy equation. Uniform nodal spacing was used in each fibrous insulation spacer region, bounded by either two foils or a foil and a solid bounding surface, while the node spacing could vary between different spacer regions. The radiant flux calculated from Eq. (4) was then used in Eq. (2) to obtain temperature distributions for the following time step.

5. RESULTS AND DISCUSSION

Typical steady-state thermal conductivity measurements are discussed and the comparison of predicted and measured thermal conductivity data is presented.

5.1 Experimental Results

The effective thermal conductivity of the four MLI samples as a function of temperature difference across the samples thickness for environmental pressure of 1.33×10^{-4} kPa and 13.3 kPa are shown in Figs. 3.a and 3.b, respectively. Error bars representing the average overall experimental uncertainty of ±7.5% are shown for sample 1.

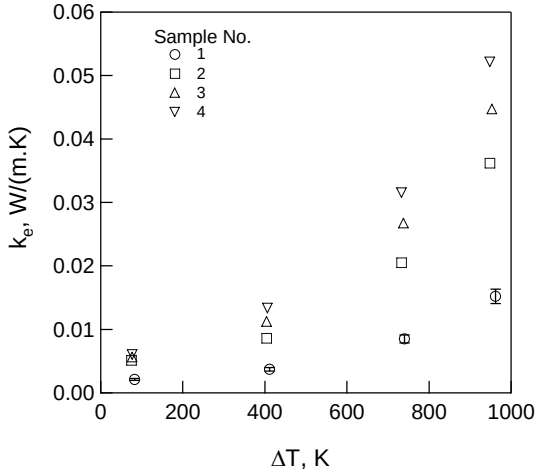

a)

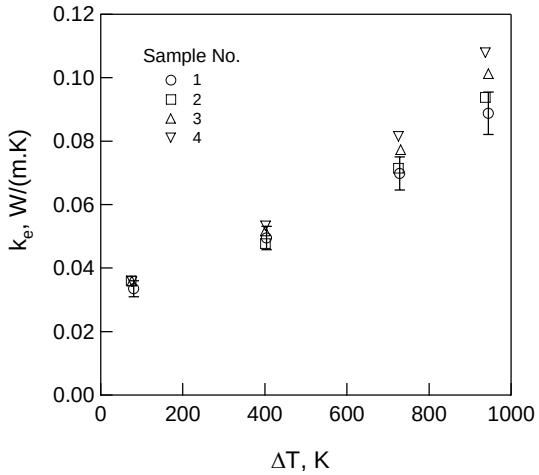

b)

Fig. 3 Variation of effective thermal conductivity with temperature difference across sample at pressures of a) 1.3×10^{-4} kPa, b) 13.3 kPa

The effective thermal conductivity varied non-linearly with temperature difference across the sample, increasing rapidly with increasing temperature due to the nonlinear nature of radiation heat transfer. At pressure of 1.33×10^{-4} kPa, gas conduction was negligible; therefore, the effective thermal conductivity comprised of contributions due to solid conduction and radiation heat transfer, with the radiation being the dominant mode of heat transfer. The 13.3 mm thick sample with 4 reflective foils (sample 1) had the lowest effective thermal conductivity, while for the 26.6 mm

thick samples the effective thermal conductivity decreased with increasing number of foils. At the nominal temperature difference of 1000 K, the effective thermal conductivity of sample 1 (13.3 mm thick with four foils) was 3.4 times lower than that of sample 4 (26.6 mm thick with one foil) at 1.3×10^{-4} kPa, but only 1.2 times lower at 13.3 kPa. At the lower pressures radiation is the dominant mode of heat transfer, and therefore, MLI, which is a radiation attenuator, provides an effective resistance to heat transfer. At high pressures, both gas conduction and radiation are significant, and therefore, the MLI is not as effective. Variation of effective thermal conductivity of the four MLI samples with environmental pressure for a nominal temperature difference of 1000 K across the sample is shown in Fig. 4.

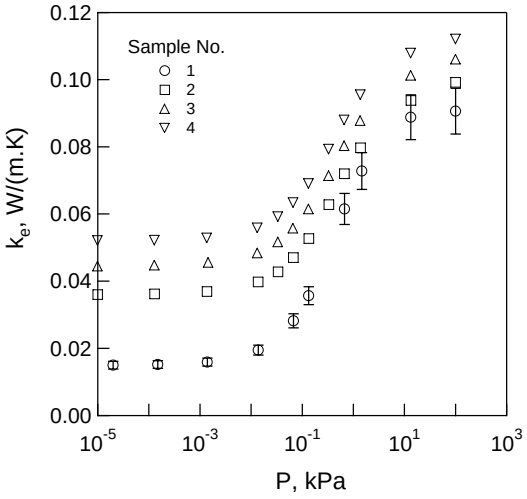

Fig. 4 Variation of effective thermal conductivity with pressure at nominal temperature difference of 1000 K

The effective thermal conductivity was essentially constant up to 1 x 10^{-3} kPa, then increased rapidly up to 13 kPa, after which it slowly increased with pressure. The difference in the effective thermal conductivity between the four samples was more significant at lower pressures in the absence of gas conduction. A comparison of the effective thermal conductivity of the three 26.6 mm thick MLI samples, sample 2 through 4, with 26.6 mm thick Saffil fibrous insulation samples [8] at densities of 48 and 72 kg/m^3 is shown in Fig. 5. The variation of effective thermal conductivity with temperature difference maintained across the sample at a pressure of 1.3×10^{-4} kPa is shown in this figure. Adding reflective foils lowered the effective thermal conductivity compared to Saffil fibrous insulation sample at the same density, 48 kg/m^3, with the effect more pronounced as temperature differences across the sample increased and as the number of foils increased. Adding one reflective foil (sample 4) resulted in a significant improvement in the effective thermal conductivity. Having two and four reflective foils (samples 3 and 2, respectively) resulted in lower effective thermal conductivies compared to Saffil at 72 kg/m^3, 1.5 times the density of the MLI samples.

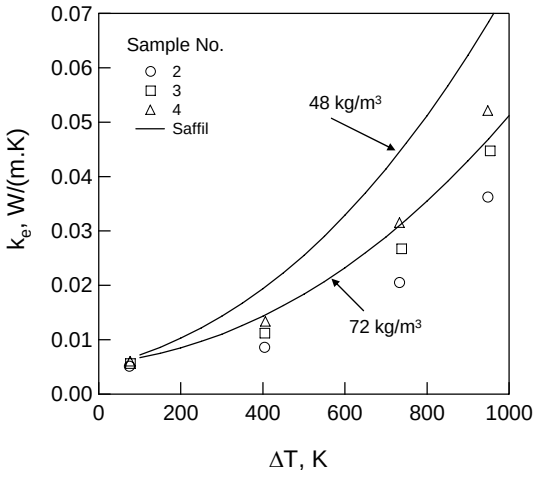

Fig. 5 Comparison of effective thermal conductivity of 26.6 mm MLI samples with Saffil at a pressure of 1.3 $\times$ 10^{-4} kPa

5.2 Validation of Numerical Model

For validating the numerical model with steady-state thermal conductivity measurements, a linearly varying initial temperature spatial distribution was used based on the measured average temperatures of the hot and cold sides of the samples from the experimental data, and then the numerical solution was marched in time until steady-state conditions were achieved. At steady state, the effective thermal conductivity was calculated from the Fourier's law of heat conduction, Eq. (1), using the calculated total steady-state heat flux (including contributions of both radiative and conductive heat fluxes) and the imposed temperature difference across the medium.

The comparison of predicted and measured effective thermal conductivities for the MLI samples at nominal pressures of 1.3 $\times10^{-2}$ and 1.4 kPa is shown in Figs. 6a and 6b, respectively, where the effective thermal conductivity is plotted versus the temperature difference maintained across the sample thickness.

The agreement between predictions and measurements were typically within the 7.5% average experimental uncertainty. Considering that the numerical predictions have certain uncertainty associated with the modified two-flux approximation and the radiant and thermal properties of the spacer and foils, the overall agreement was satisfactory. The agreement was not as good at the

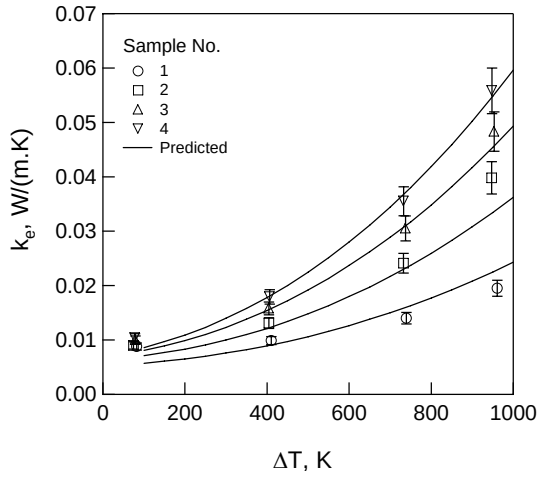

a)

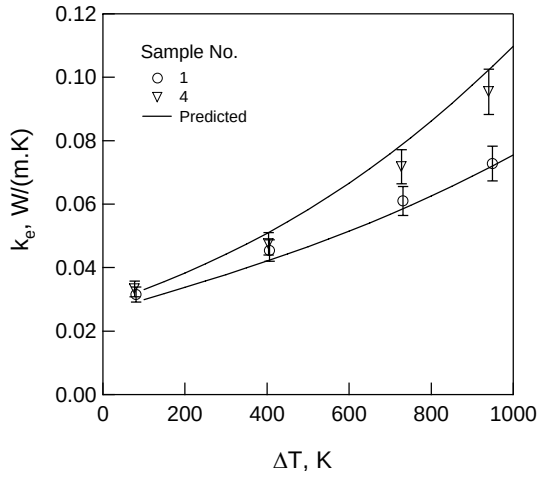

b)

Fig. 6. Comparison of measured and predicted effective thermal conductivity at pressures of a) 0.013 kPa, b) 1.4 kPa

lowest pressures $1.3 \times 10^{-5} - 1.3 \times 10^{-3}$ kPa. At these pressures the main mechanism for heat transfer was radiation, therefore, the overall numerical predictions were more sensitive to any uncertainties in the radiation modeling and radiant properties of the spacers and foils. Furthermore, the measurement uncertainties were higher compared to the reported average overall uncertainty for the cases at the lower pressures and temperatures. Percent root mean square (RMS) deviations between experimental and predicted effective thermal conductivities were 11.1, 12.7, 7.5, and 5.4, for samples 1, 2, 3, and 4, respectively, with an overall percent RMS deviation of 9.5.

6. CONCLUDING REMARKS

The combined radiation/conduction heat transfer in high-temperature multilayer insulations was investigated experimentally and numerically. The steady-state heat transfer through four multilayer insulation configurations was investigated experimentally over the temperature range of 300-1300 K and environmental pressure range of 1.33×10^{-5}-101.32 kPa. It was shown that including the reflective foils reduced the effective thermal conductivity compared to fibrous insulation samples. Using two or four foils resulted in lower effective thermal conductivities compared to using fibrous insulation at 1.5 times the density of the multilayer insulations. A finite volume numerical model was developed to solve the governing combined radiation/ conduction heat transfer equations. The radiation heat transfer in the fibrous insulation spacers was modeled using the modified two-flux approximation assuming anisotropic scattering and gray medium. The numerical model was validated by comparison with steady-state experimental data. The overall root mean square deviation between the predicted and measured effective thermal conductivity of the samples was 9.5%.

7. REFERENCES

1. Dotts, R. L., Curry, D. M., and Tillian, D. J., "Orbiter Thermal Protection System," Space Shuttle Technology Conference Proceedings, Part 2, 1985, pp. 1062-1081.

2. Alloway, R., "X-33 Metallic Thermal Protection System," NASA CR-2003-212662, November 2003.

3. Blosser, M. L., Chen, R. R., Schmidt, I. H., Dorsey, J. T., Poteet, C. C., Bird, R. K., and Wurster, K. E., "Development of Advanced Metallic Thermal-Protection-System Prototype Hardware," *Journal of Spacecraft and Rockets*, Vol. 41, No. 2, 2004, pp. 183-19,

4. Grallert, H., and Keller, K., "Metallic Thermal Protection Concept for Hypersonic Vehicles," *Journal of Aircraft*, Vol. 28, No. 6, 1991, pp. 410- 416.

5. Hald, H., Petersen, D., Reimer, T., Rühle, F., Winkelmann, P. , and Weihs, H., "Development of a CMC-Based TPS for Two Representative Specimens of Cryogenic Tank RLV's," AIAA 98-1609, 1998.

6. Donabedian, M., and Gilmore, D. G., "Multilayer Insulation and Barriers," *Satellite Thermal Control Handbook*, Ch. 4, Section 3, Ed. by D. G. Gilmore, The Aerospace Corporation Press, 1994.

7. Cunnington, G. R., and Tien, C. L., "A Study of Heat-transfer Process in Multilayer Insulations," AIAA 69-607, 1969.

8. Daryabeigi, K., "Heat Transfer in High-Temperature Fibrous Insulation," *Journal of Thermophysics and Heat Transfer*, Vol. 17, No. 1, 2003, pp. 10-20.

9. Cunnington, G. R., Zierman, C. A., Funai, A., and Lindahn, A., "Performance of Multilayer Insulation Systems for Temperatures to 700K," NASA CR-907, October 1967.

10. DeWitt, W. D., Gibbon, R. L., and Reid, R. L., "Multi-foil Type Thermal Insulation," *Intersociety Energy Conversion Engineering Conference Record,* Institute of Electrical and Electronics Engineers, New York, 1968, pp. 263-271.

11. Mühlratzer, A., Handrick, K., and Weber, K.-H., "Hermes Thermal Protection System Internal Multilayer Insulation (IMI)," International Astronautical Federation (IAF) Paper 90-282, October 1990.

12. Keller, K., Blumenberg, J., and Tomsik, J., "Fibre Orientation and the Conduction of Heat by a Gas Enclosed in Ceramic Layers," *Journal of Flight Sciences and Space Research*, Vol. 12, No. 4, 1988, pp. 258-260.

13. Keller, K., Hoffmann, M., Zörner, W., and Blumenberg, J., "Application of High Temperature Multilayer Insulations," *Acta Astronautica*, Vol. 26, No. 6, 1992, pp. 451-458.

14. Stauffer, T., Jog, M., and Ayyaswamy, P., "The Effective Thermal Conductivity of Multi Foil Insulation as a Function of Temperature and Pressure," AIAA Paper 92-2939, July 1992.

15. Daryabeigi, K., "Thermal Analysis and Design of Multilayer Insulation for Reentry Aerodynamic Heating," *Journal of Spacecraft and Rockets*, Vol. 39. No. 4, 2002, pp. 509-514.

16. Daryabeigi, K, "Effective Thermal Conductivity of High Temperature Insulations for Reusable Launch Vehicles," NASA TM-1999-208972, Feb. 1999.

17. "Standard Test Method for Thermal Conductivity of Refractories," *Annual Book of ASTM Standards*, Vol. 15.01, American Society for Testing and Materials, West Conshohocken, PA, 2000, pp. 54-59.

18. Sparrow, E. M., and Cess, R. D., *Radiation Heat Transfer*, Augmented Ed., 1978, McGraw-Hill, New York, 1978, pp. 255-271.

19. Domoto, G. A. and Wang, W. C., "Radiative Transfer in Homogeneous Nongray Gases with Nonisotropic Particle Scattering," *Journal of Heat Transfer*, Vol. 96, August 1974, pp. 385-390.

20. Matthews, L. K., Viskanta, R., and Incropera, F. P., "Combined Conduction and Radiation Heat Transfer in Porous Materials Heated by Intense Solar Radiation," *Journal of Solar Energy Engineering*, Vol. 107, February 1985, pp. 29-34.

21. Marschall, J., Maddren, J., and Parks, J., "Internal Radiation Transport and Effective Thermal Conductivity of Fibrous Ceramic Insulation," AIAA 2001-2822, June 2001.

22. Siegel, R., and Howell, J. R., *Thermal Radiation Heat Transfer*, 2nd Ed., McGraw-Hill, New York, 1981, pp. 426-427.

23. Gebhart, B., *Heat Conduction and Mass Diffusion*, McGraw-Hill, New York, 1993, pp. 442-444.

24. Williams, S. D., and Curry, D. M., "Predictions of Rigid Silica Based Insulation Conductivity," NASA TP-3276, January 1993.